Biomedical Optics EXPRESS

Simultaneous assessment of red blood cell aggregation and oxygen saturation under pulsatile flow using high-frequency photoacoustics

Tae-Hoon Bok, Eno Hysi, and Michael C. Kolios*

Department of Physics, Ryerson University, 350 Victoria Street, Toronto, Ontario, M5B 2K3 Institute for Biomedical Engineering, Science and Technology (iBEST), a partnership between Ryerson University and St. Michael's Hospital, 209 Victoria Street, Toronto, Ontario, M5B 1T8, Canada

**mkolios@ryerson.ca*

Abstract: We investigate the feasibility of photoacoustic (PA) imaging for assessing the correlation between red blood cell (RBC) aggregation and the oxygen saturation (sO_2) in a simulated pulsatile blood flow system. For the 750 and 850 nm illuminations, the PA amplitude (PAA) increased and decreased as the mean blood flow velocity decreased and increased, respectively, at all beat rates (60, 120 and 180 bpm). The sO_2 also cyclically varied, in phase with the PAA for all beat rates. However, the linear correlation between the sO_2 and the PAA at 850 nm was stronger than that at 750 nm. These results suggest that the sO_2 can be correlated with RBC aggregation induced by decreased mean shear rate in pulsatile flow, and that the correlation is dependent on the optical wavelength. The hemodynamic properties of blood flow assessed by PA imaging may be used to provide a new biomarker for simultaneous monitoring blood viscosity related to RBC aggregation, oxygen delivery related to the sO_2 and their clinical correlation.

OCIS codes: (110.5125) Photoacoustics; (170.1470) Blood or tissue constituent monitoring.

References and links

1. K. R. Walley, "Use of central venous oxygen saturation to guide therapy," Am. J. Respir. Crit. Care Med. **184**(5), 514–520 (2011).
2. J. V. Pope, A. E. Jones, D. F. Gaieski, R. C. Arnold, S. Trzeciak, and N. I. Shapiro; Emergency Medicine Shock Research Network (EMShockNet) Investigators, "Multicenter study of central venous oxygen saturation (ScvO2) as a predictor of mortality in patients with sepsis," Ann. Emerg. Med. **55**(1), 40–46 (2010).
3. A. E. Jones, N. I. Shapiro, S. Trzeciak, R. C. Arnold, H. A. Claremont, and J. A. Kline; Emergency Medicine Shock Research Network (EMShockNet) Investigators, "Lactate clearance vs central venous oxygen saturation as goals of early sepsis therapy: a randomized clinical trial," JAMA **303**(8), 739–746 (2010).
4. B. Chance, E. Borer, A. Evans, G. Holtom, J. Kent, M. Maris, K. McCully, J. Northrop, and M. Shinkwin, "Optical and nuclear magnetic resonance studies of hypoxia in human tissue and tumors," Ann. N. Y. Acad. Sci. **551**(1 Membrane in C), 1–16 (1988).
5. H. Liu, D. A. Boas, Y. Zhang, A. G. Yodh, and B. Chance, "Determination of optical properties and blood oxygenation in tissue using continuous NIR light," Phys. Med. Biol. **40**(11), 1983–1993 (1995).
6. G. Mardirossian and R. E. Schneider, "Limitations of pulse oximetry," Anesth. Prog. **39**(6), 194–196 (1992).
7. X. Wang, X. Xie, G. Ku, L. V. Wang, and G. Stoica, "Noninvasive imaging of hemoglobin concentration and oxygenation in the rat brain using high-resolution photoacoustic tomography," J. Biomed. Opt. **11**(2), 024015 (2006).
8. L. Wang, K. Maslov, and L. V. Wang, 8. L. Wang, K. Maslov, and L. V Wang, "Single-cell label-free photoacoustic flowoxigraphy in vivo," Proc. Natl. Acad. Sci. United State Am. (2013).
9. H. F. Zhang, K. Maslov, M. Sivaramakrishnan, G. Stoica, and L. V. Wang, "Imaging of hemoglobin oxygen saturation variations in single vessels in vivo using photoacoustic microscopy," Appl. Phys. Lett. **90**(5), 053901 (2007).

#262587 Received 5 Apr 2016; revised 13 Jun 2016; accepted 14 Jun 2016; published 23 Jun 2016

10. H. F. Zhang, K. Maslov, G. Stoica, and L. V. Wang, "Functional photoacoustic microscopy for high-resolution and noninvasive in vivo imaging," Nat. Biotechnol. **24**(7), 848–851 (2006).
11. F. T. H. Yu, J. K. Armstrong, J. Tripette, H. J. Meiselman, and G. Cloutier, "A local increase in red blood cell aggregation can trigger deep vein thrombosis: evidence based on quantitative cellular ultrasound imaging," J. Thromb. Haemost. **9**(3), 481–488 (2011).
12. Q. Li, L. Li, and Y. Li, "Enhanced RBC aggregation in type 2 diabetes patients," J. Clin. Lab. Anal. **29**, 387–389 (2014).
13. T.-H. Bok, Q. Kong, K.-H. Nam, Y. H. Oh, J. G. Kim, J. J. Lee, J. C. Choi, and D.-G. Paeng, 13. T.-H. Bok, Q. Kong, K.-H. Nam, Y. H. Oh, J. G. Kim, J. J. Lee, J. C. Choi, and D.-G. Paeng, "A pilot study of blood echogenicity from the radial artery and the carotid artery of stroke patients," in *Proceedings of IEEE International Ultrasonics Symposium* (Institute of Electrical and Electronics Engineers, New York, 2012), pp. 2364–2367.
14. O. K. Baskurt and H. J. Meiselman, "Erythrocyte aggregation: basic aspects and clinical importance," Clin. Hemorheol. Microcirc. **53**(1-2), 23–37 (2013).
15. G. Erikssen, K. Liestøl, J. V. Bjørnholt, H. Stormorken, E. Thaulow, and J. Erikssen, "Erythrocyte sedimentation rate: a possible marker of atherosclerosis and a strong predictor of coronary heart disease mortality," Eur. Heart J. **21**(19), 1614–1620 (2000).
16. B. S. Bull and J. D. Brailsford, "The zeta sedimentation ratio," Blood **40**(4), 550–559 (1972).
17. D. E. Brooks, J. W. Goodwin, and G. V. F. Seaman, "Rheology of erythrocyte suspensions: electrostatic factors in the dextran-mediated aggregation of erythrocytes," Biorheology **11**(1), 69–77 (1974).
18. G. Cloutier and Z. Qin, "Ultrasound backscattering from non-aggregating and aggregating erythrocytes--a review," Biorheology **34**(6), 443–470 (1997).
19. M. R. Hardeman, J. G. G. Dobbe, and C. Ince, "The Laser-assisted Optical Rotational Cell Analyzer (LORCA) as red blood cell aggregometer," Clin. Hemorheol. Microcirc. **25**(1), 1–11 (2001).
20. Y. Li, T.-H. Bok, J. H. Yang, M. J. Choi, and D.-G. Paeng, "The Acute Effects of Smoking on the Cyclic Variations in Blood Echogenicity of Carotid Artery," Ultrasound Med. Biol. **37**(4), 513–521 (2011).
21. D.-G. Paeng, K.-H. Nam, and K. K. Shung, "Cyclic and radial variation of the echogenicity of blood in human carotid arteries observed by harmonic imaging," Ultrasound Med. Biol. **36**(7), 1118–1124 (2010).
22. N. Tateishi, Y. Suzuki, I. Cicha, and N. Maeda, "O_2 release from erythrocytes flowing in a narrow O_2-permeable tube: effects of erythrocyte aggregation," Am. J. Physiol. Hear. Circ. Physiol. **281**, H448–H456 (2001).
23. N. Tateishi, Y. Suzuki, M. Shirai, I. Cicha, and N. Maeda, "Reduced oxygen release from erythrocytes by the acceleration-induced flow shift, observed in an oxygen-permeable narrow tube," J. Biomech. **35**(9), 1241–1251 (2002).
24. E. Hysi, R. K. Saha, and M. C. Kolios, "On the use of photoacoustics to detect red blood cell aggregation," Biomed. Opt. Express **3**(9), 2326–2338 (2012).
25. E. Hysi, R. K. Saha, and M. C. Kolios, "Photoacoustic ultrasound spectroscopy for assessing red blood cell aggregation and oxygenation," J. Biomed. Opt. **17**(12), 125006 (2012).
26. A. Needles, A. Heinmiller, J. Sun, C. Theodoropoulos, D. Bates, D. Hirson, M. Yin, and F. S. Foster, "Development and initial application of a fully integrated photoacoustic micro-ultrasound system," IEEE Trans. Ultrason. Ferroelectr. Freq. Control **60**(5), 888–897 (2013).
27. R. K. Saha and G. Cloutier, "Monte Carlo study on ultrasound backscattering by three-dimensional distributions of red blood cells," Phys. Rev. E Stat. Nonlin. Soft Matter Phys. **78**(6), 061919 (2008).
28. G. J. Diebold, 28. G. J. Diebold, "Photoacoustic Monopole Radiation: Waves from Objects with Symmetry in One, Two, and Three Dimensions," in *Photoacoustic Imaging and Spectroscopy*, L. V Wang, ed. (CRC Press, 2009), pp. 3–17.
29. M. Eriksen, "Effect of pulsatile arterial diameter variations on blood flow estimated by Doppler ultrasound," Med. Biol. Eng. Comput. **30**(1), 46–50 (1992).
30. G. W. Snedecor and W. G. Cochran, *Statistical Methods* (Iowa State University Press, 1989).
31. S. Prahl, 31. S. Prahl, "Optical Absorption of Hemoglobin," http://omlc.org/spectra/hemoglobin/ (2015).
32. T.-H. Bok, Y. Li, K.-H. Nam, J. C. Choi, and D.-G. Paeng, "Feasibility study of high-frequency ultrasonic blood imaging in human radial artery," J. Med. Biol. Eng. **35**(1), 21–27 (2015).
33. C.-C. Huang, "Cyclic variations of high-frequency ultrasonic backscattering from blood under pulsatile flow," IEEE Trans. Ultrason. Ferroelectr. Freq. Control **56**(8), 1677–1688 (2009).
34. C.-C. Huang, C.-C. Liao, P.-Y. Lee, and C.-C. Shih, "The effect of flow acceleration on the cyclic variation of blood echogenicity under pulsatile flow," Ultrasound Med. Biol. **39**(4), 670–680 (2013).
35. K.-H. Nam, T.-H. Bok, Q. Kong, and D.-G. Paeng, "High spatial and temporal resolution observations of pulsatile changes in blood echogenicity in the common carotid artery of rats," Ultrasound Med. Biol. **39**(9), 1665–1671 (2013).
36. A. B. Rowley, S. J. Payne, I. Tachtsidis, M. J. Ebden, J. P. Whiteley, D. J. Gavaghan, L. Tarassenko, M. Smith, C. E. Elwell, and D. T. Delpy, "Synchronization between arterial blood pressure and cerebral oxyhaemoglobin concentration investigated by wavelet cross-correlation," Physiol. Meas. **28**(2), 161–173 (2007).
37. T. Peng, P. N. Ainslie, J. D. Cotter, C. Murrell, K. Thomas, M. J. A. Williams, K. George, R. Shave, A. B. Rowley, and S. J. Payne, "The effects of age on the spontaneous low-frequency oscillations in cerebral and systemic cardiovascular dynamics," Physiol. Meas. **29**(9), 1055–1069 (2008).

#262587 Received 5 Apr 2016; revised 13 Jun 2016; accepted 14 Jun 2016; published 23 Jun 2016

38. Z. Li, Y. Wang, Y. Li, Y. Wang, J. Li, and L. Zhang, "Wavelet analysis of cerebral oxygenation signal measured by near infrared spectroscopy in subjects with cerebral infarction," Microvasc. Res. **80**(1), 142–147 (2010).
39. Z. Li, M. Zhang, Q. Xin, S. Luo, R. Cui, W. Zhou, and L. Lu, "Age-related changes in spontaneous oscillations assessed by wavelet transform of cerebral oxygenation and arterial blood pressure signals," J. Cereb. Blood Flow Metab. **33**(5), 692–699 (2013).

1. Introduction

Red blood cells (RBCs) are mainly involved in the transport and exchange of physiologically relevant gasses. The transport of oxygen is governed by the blood oxygen saturation (sO_2) [1], a measure of the RBC's oxygen carrying capacity. The clinical significance of sO_2 has been well established making measurements of sO_2 a routine physiological parameter in the emergency and operating rooms [2,3]. The measurement of the sO_2 has been traditionally conducted by optical spectroscopy [4,5] but it is limited by the penetration depth and lack of spatial resolution of conventional optical imaging techniques. Additionally, pulse oximetry readings are prone to error as a result of hypotension, hypothermia, muscular twitching, dyshemoglobinnemias and body movements [6]. Over the past decade, the sO_2 measurement methods have been significantly improved through advances in photoacoustic (PA) imaging [7–10]. However, these previous studies have focused on the sO_2 measurement by PA imaging in micron-diameter vessels without considering hemodynamic and/or hemorheological effects such as RBC aggregation.

RBCs become aggregated when flowing blood is exposed to stasis or very low shear rate conditions. RBC aggregation is a hemodynamic and hemorheological phenomenon which is manifested at enhanced rates in various pathologies such as deep vein thrombosis [11], diabetes [12] or strokes [13]. In addition, RBC aggregation is known to alter blood viscosity which affects blood flow dynamics, vascular resistance and tissue perfusion [14]. The measurement of RBC aggregation has been widely studied using several biophysical techniques including erythrocyte sedimentation rate [15], centrifugation methods [16], low shear viscometry [17], ultrasound (US) imaging [18] and analysis of light transmission or reflection of RBC suspensions [19]. Among these methods, US imaging provides the most non-invasive method to measure RBC aggregation [18,20,21]. In addition, US imaging studies have also quantified RBC aggregation under blood flow. However, US imaging is not capable of assessing oxygen delivery, the main functional role of RBCs.

RBC aggregation and the sO_2 are intrinsically related phenomena since they are dependent on the hemodynamics and biochemistry of RBCs. Therefore, the relationship between RBC aggregation and the sO_2 may provide a new biomarker for disorders where aggregation becomes pathological. Tateishi et al. [22,23] have reported that the diffusion of oxygen from RBCs is inhibited by aggregation and partly due to the thickening of the cell-free layer. However, in their work, they demonstrated the correlation between the sO_2 and RBC aggregation induced by Dextran T-70, not by a flow induced hemodynamic parameter such as shear rate. In previous studies by our group [24,25], the PA measurement of RBC aggregation and the sO_2 was preliminarily conducted under the static conditions using Dextran. In order to further advance the clinical applicability of PA imaging, the relationship between RBC aggregation and the sO_2 should be investigated simultaneously under flowing conditions.

In this paper, high-frequency PA imaging is proposed to simultaneously assess RBC aggregation and the sO_2 under pulsatile blood flow. The pulsatile blood flow was generated by varying the beat rate (60, 120 and 180 bpm) within a flow phantom. The flowing blood was imaged at two optical illumination wavelengths for estimating the sO_2 using a high-frequency PA system. This paper aims to examine the relationship between hemodynamic parameters that control blood flow and sO_2 estimates using PA imaging. We hypothesize that the relationship between the PA amplitude (PAA) and the sO_2 will be dependent on the optical wavelength and will provide insights related to RBC aggregation and the sO_2.

#262587 Received 5 Apr 2016; revised 13 Jun 2016; accepted 14 Jun 2016; published 23 Jun 2016

2. Materials and methods

2.1 Blood source

Human whole blood was collected by netCAD (Vancouver, BC, Canada), the research division of Canadian Blood Services, under protocol 2013-001 which involves standard Canadian Blood Services collection and testing procedures of whole blood. It was delivered overnight at 4°C, with continuous monitoring during shipment to ensure no temperature deviations occur. The procedures for using the blood have been approved by the research ethics boards of Ryerson University and the Canadian Blood Services. Whole blood units from three different volunteers were used in order to ensure the repeatability of experimental results.

2.2 Blood flow system and US/PA imaging

A simulated blood flow system was developed using a peristaltic pump (MasterFlex, Cole-Parmer, Montreal, QC, Canada), a silicone tube, a triangle beaker, and a 2-mm-diameter flow phantom made from porcine skin gelatin (Sigma Aldrich, Oakville, ON, Canada) at a concentration of 15% wt/vol in degassed water (Fig. 1). The silicone tube and beaker were used for circulating blood and as a reservoir, respectively. The blood in the reservoir was stirred by the spin bar in order to prevent RBCs from sedimentation, and was kept as 35 °C by the hot plate. The entrance of the reservoir which two tubes were inserted was sealed in order to minimize the exposure of blood to the surrounding air. Beat rates of 60, 120 and 180 bpm were generated within the phantom by the peristaltic pump. The vessel diameter extended and contracted periodically at the intervals corresponding to the beat rate, and the expansion of the diameter increased with the beat rate. The effect of the vessel lumen expansion on the PAA could be ignored since the PA signals were due to RBCs and their aggregation. In addition, the PAA was averaged in the region of interest, so that the increased blood volume under high pressure could be considered negligible.

A representative, co-registered US/PA image of flowing blood is shown in Fig. 1. The image was acquired using a commercialized US/PA system equipped with a 40 MHz, 256 elements linear-array probe (VevoLAZR; LZ550, FUJIFILM VisualSonics, Toronto, ON, Canada) [26]. The coaxial US cable and the optical fiber bundle were integrated into a special enclosure. The fiber bundle (fused borosilicate fiber, 7.5mm in diameter at input, 0.55 numerical aperture) is coupled to a tunable Nd:YAG laser which was operated through an optical parametric oscillator which outputted wavelengths between 680 and 970 nm (10 ns pulse length, 30 mJ/pulse, 20 Hz repetition rate). The output of the fiber was emitted from two rectangular strips on both sides of the acoustic aperture as an ellipsoid on a 30° angle (0.58 rad major/minor divergence in air) relative to the imaging plane. PA measurements were performed for three blood samples, three beat rates (60, 120 and 180 bpm), and two optical wavelengths (750 and 850 nm). The same measurement was performed for 800 nm at 60 bpm in order to consider an isosbestic point. For each measurement, 200 US/PA B-mode frames were recorded corresponding to a measurement time of 10 seconds. Out of the 200 frames, the 160 frames corresponding to 8 seconds (20 Hz acquisition rate) were extracted and synchronized to the initial phase of each measurement.

#262587 Received 5 Apr 2016; revised 13 Jun 2016; accepted 14 Jun 2016; published 23 Jun 2016

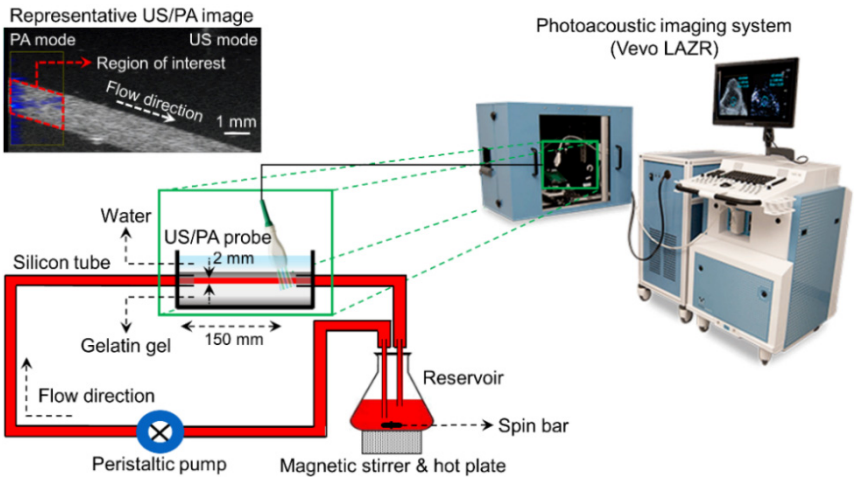

Fig. 1. Experimental set-up of the blood flow and photoacoustic imaging system along with a representative US/PA image.

2.3 Simultaneous assessment of RBC aggregation, sO_2, and shear rate

RBCs become aggregated when flowing blood is subject to very low shear rates. Even though the RBCs are biconcave in shape, for the purposes of simulating aggregation at these photoacoustic detection frequencies, they can be approximated as spheres to represent the formation of clusters of aggregates [27]. The PAA from RBC aggregates can be approximated as the PAA from a sphere (P_s) as described in Eq. (1) [28].

$$p_s(\hat{\tau}) = \frac{i\mu_a \beta F v_s^2 a}{2\pi C_p r} \int_{-\infty}^{\infty} \frac{(\sin\hat{q} - \hat{q}\cos\hat{q}) e^{-i\hat{q}\hat{\tau}}}{\hat{q}^2 \left[(1-\hat{\rho})(\sin\hat{q})/\hat{q} - \cos\hat{q} + i\hat{q}\hat{v}\sin\hat{q}\right]} d\hat{q} \tag{1}$$

where μ_a is the optical absorption coefficient, β is the isobaric thermal expansion coefficient, F is the optical fluence of the excitation light, v_s is the sound speed in the absorber, a is the radius of uniformly irradiated sphere, C_p is the heat capacity per unit mass, r is the distance between the absorber and the ultrasonic detector, $\hat{q}$ is defined as $\hat{q} = \omega\ a / v_s$ where ω is the modulation frequency of the optical beam, $\hat{\tau}$ is the dimensionless retarded time from the edge of the sphere defined as $\hat{\tau} = (v_s/a)[t-(r-a)/v_f]$ where v_f is the sound speed in the surrounding fluid medium, $\hat{\rho} = \rho_s/\rho_f$ and $\hat{v} = v_s/v_f$ are the ratios of density and the sound speed, respectively, where ρ_s and ρ_f are the density of the absorber and the surrounding fluid medium, respectively. The PAA from aggregating blood is mainly governed by a related to the aggregate size. Hence, the formation of RBC aggregation can be assessed by the changes in the PAA.

The sO_2 was estimated by computing the ratio of oxygenated hemoglobin (HbO) to the total hemoglobin. It was assumed that HbO and deoxygenated hemoglobin (Hb) were the dominant absorbers at the two optical illumination wavelengths λ_1 and λ_2, and was computed by [7]

$$\mu_a^{\lambda} = \varepsilon_{\mathrm{HbO}}^{\lambda}[\mathrm{HbO}] + \varepsilon_{\mathrm{Hb}}^{\lambda}[\mathrm{Hb}] \tag{2}$$

$$\mathrm{sO}_2 = \frac{[\mathrm{HbO}]}{[\mathrm{HbO}]+[\mathrm{Hb}]} = \frac{\mu_a^{\lambda_2}\varepsilon_{\mathrm{Hb}}^{\lambda_1} - \mu_a^{\lambda_1}\varepsilon_{\mathrm{Hb}}^{\lambda_2}}{\mu_a^{\lambda_1}(\varepsilon_{\mathrm{HbO}}^{\lambda_2} - \varepsilon_{\mathrm{Hb}}^{\lambda_2}) - \mu_a^{\lambda_2}(\varepsilon_{\mathrm{HbO}}^{\lambda_1} - \varepsilon_{\mathrm{Hb}}^{\lambda_1})} \tag{3}$$

where [HbO] and [Hb] are the molar concentrations of HbO and Hb, respectively; μ_a is equal to $P/(\Gamma \cdot F)$ where P is the detected PA pressure, and Γ is the Gruneisen parameter, so that P is

#262587 Received 5 Apr 2016; revised 13 Jun 2016; accepted 14 Jun 2016; published 23 Jun 2016

used instead of the μ_a in order to compute the sO_2 assuming that Γ and F are constant; and ε_{HbO} and ε_{Hb} are the known molar extinction coefficients of HbO and Hb, respectively. The energy of each pulse at both wavelengths of illumination was taken into account, while fluence corrections were not applied to the PA estimations of sO_2. An energy meter (Vega, Ophir-Spiricon, North Logan, UT, USA) was used to monitor the wavelength-dependent energy variations, and the measured energy was used to normalize the PA signals at each respective wavelength. Within the scope of the current study and given that the vessel diameter was only 2 mm, the object of interest was the relative variations in the sO_2 due to the presence of RBC aggregation rather than an absolute value of the sO_2.

Ideally, the blood flow velocity (BFV) should be simultaneously measured as the PA images are acquired in order to interpret the relationship between RBC aggregation, the sO_2 and the shear rate. The shear rate can be related to the radial gradient of the laminar flow velocity in a cylindrical tube. The PA system, however, was limited in the ability to measure PA signals and blood flow velocities simultaneously. In lieu of that, the mean BFV (mBFV) within the region of interest shown in Fig. 1 was measured by pulsed wave Doppler (Doppler angle: 55°, pulse repetition frequency: 75 kHz) for the same duration as each PA image. The radial profile of the velocity of the non-Newtonian steady flow is parabolic in 2 dimensions, so that the shear rate is dependent on the radial position. To simplify the calculation, the mean shear rate can be used as a kinetic factor of RBC aggregation, and the mBFV (proportional to the mean shear rate) was used as an alternative kinetic factor of RBC aggregation in this paper. The maximum and minimum of the mBFV were assumed to be synchronized with the maximum and minimum of the vessel diameter since the vessel expands and contracts during systole and diastole, respectively [29].

The aforementioned measurement parameters could then be synchronized since the PA image provided the PAA (associated with RBC aggregation in the vessel lumen), the sO_2 (from two optical wavelengths), and the mBFV using Doppler imaging and synchronized using the vessel diameter. In order to quantify the variation of the measurement parameters, the variation index (VI, %) and the magnitude of cyclic variation (Δ) were computed by

$$\mathrm{VI}_X = \frac{1}{N}\sum_{n=1}^{N}\left(\frac{X_{\max}}{X_{\min}} - 1\right)\times 100\Big|_{T_n}, \qquad \Delta Y = \frac{1}{N}\sum_{n=1}^{N}(Y_{\max} - Y_{\min})\Big|_{T_n} \tag{4}$$

where X is the PAA, N is the number of cycles (N = 8, 16 and 24 for 60, 120 and 180 bpm, respectively), T_n is the order of cycle, Y is the sO_2, the mBFV and the computed μ_a, and the subscripts max and min indicate the maximum and minimum values.

2.4 Optical wavelength dependency on the correlation between RBC aggregation and sO_2

The relationship between RBC aggregation and sO_2 can be estimated by the relationship between the PAA and sO_2. The PAA at 750 and 850 nm were obtained by the aforementioned methods, and the sO_2 was computed using Eq. (2). Simultaneous measurements of the PAA and the sO_2 were plotted for both optical wavelengths. The PAA and the sO_2 values were derived from 160 recordings during an 8 s time interval (as the frame rate was 20 Hz). The 95% confidence ellipses of the 160 data points were computed for both wavelengths in order to compute the eigenvalues of the covariance (i.e. axes of the ellipse) [30]. In addition, PA measurements were also performed at 800 nm, the isosbestic wavelength where the absorption of oxygenated and deoxygenated Hb is identical. This was done in order to investigate the origin of the PAA variations in the absence of any oxygen-dependent changes in absorption.

Even if the PAA increases with RBC aggregation, the variation of the PAA at 750 nm would be different from that at 850 nm since ε_{HbO} and ε_{Hb} are dependent on the optical wavelength [31]. The correlation between the PAA and the sO_2 can be explained by the molar extinction coefficients of HbO (ε_{HbO}) and Hb (ε_{Hb}). As shown by Eq. (2), the μ_a of RBC (and therefore a collection of RBCs in blood) is a function of ε_{HbO}, ε_{Hb}, [HbO] and [Hb]. The ε_{HbO}

#262587 Received 5 Apr 2016; revised 13 Jun 2016; accepted 14 Jun 2016; published 23 Jun 2016

and ε_{Hb} at 750 and 850 nm are well known parameters for both oxygenated and deoxygenated blood [31]. Examination of Eq. (3) reveals that the sO_2 is directly proportional to the concentration of oxygenated hemoglobin, [HbO]. The concentration of deoxygenated hemoglobin [Hb] can be approximated by 1-sO_2. The μ_a of any RBC sample can then be converted into

$$\mu_a^{\lambda} \approx (\varepsilon_{HbO}^{\lambda} - \varepsilon_{Hb}^{\lambda})\, sO_2 + \varepsilon_{Hb}^{\lambda} \tag{5}$$

where ε_{HbO} and ε_{Hb} are 518 and 1,405.24 /cm/M at 750 nm, and are 1,058 and 691.32 /cm/M at 850 nm, respectively [31]. The μ_a of the blood samples at 750 and 850 nm were computed based on Eq. (5).

3. Results and discussion

3.1 PAA and sO_2 vs. BFV

The representative images of the PAA at both the peak-systolic luminal expansion and the end-diastolic luminal contraction at all beat rates were shown in Fig. 2-top. The overall image brightness decreased during the peak-systolic luminal expansion and returned strong in the phase of the end-diastolic luminal contraction. The PAA at 750 and 850 nm and the mBFV varied periodically for all beat rates, as shown in Fig. 2-center & bottom. The mean shear rate of blood flow is directly proportional to the mBFV. Therefore, cyclical changes in the mBFV can be used to infer changes in the mean shear rate and hence changes in RBC aggregation. The dominant source of the PA signal in blood samples are the RBCs, as shown from our previous work [24,25]. The cyclic variation in the PAA is induced by the RBC aggregation and disaggregation that occurs repeatedly at different phases of the flow cycle, being similarly consistent with the cyclic variation in the US amplitude as shown in Fig. 3. The cyclic variation in the US amplitude due to RBC aggregation was widely reported [13,20,21,32–35]. The spatiotemporal correlation between the increase in the PA and US amplitudes with the formation of aggregates suggests that PA imaging is also sensitive to the dynamic changes in RBC aggregation during pulsatile flow. The cyclical variations in the mBFV and PAA are out of phase each other. The US amplitude phase is identical to the PAA for all beat rates. This phase reversal is caused by the fact that RBCs aggregate when the mean shear rate decreases. This is consistent with what has been observed using high frequency US imaging.

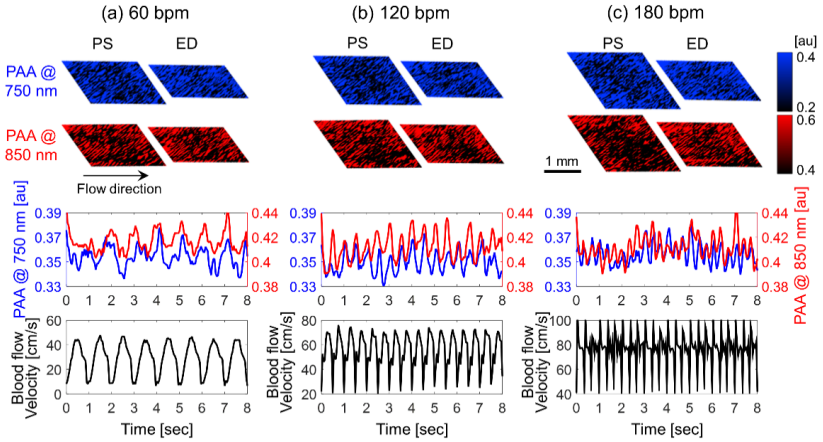

Fig. 2. Representative images of the photoacoustic amplitude (PAA) at the peak-systolic luminal expansion (PS) and the end-diastolic luminal contraction (ED) (top row). Cyclic variation in the photoacoustic amplitude (PAA) at 750 (blue line) and 850 (red line) nm (center row) and the mean blood flow velocity (bottom row). The left, center and right columns represent 60 (a), 120 (b) and 180 (c) bpm.

#262587 Received 5 Apr 2016; revised 13 Jun 2016; accepted 14 Jun 2016; published 23 Jun 2016

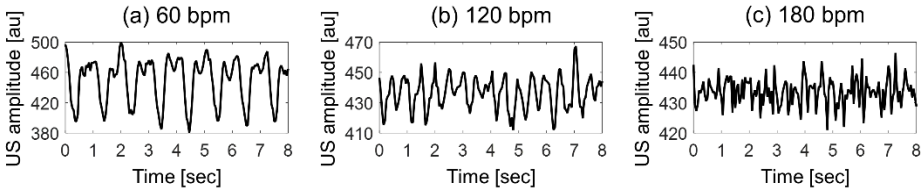

Fig. 3. Cyclic variation in the ultrasound (US) amplitude at 60 (a), 120 (b) and 180 (c) bpm.

In order to examine the advantage of PA imaging of RBC aggregation to the US counterpart, oxygen saturation maps were constructed using the two-wavelength approach. Representative images of the sO_2, estimated by using Eq. (3), at the peak-systolic luminal expansion and the end-diastolic luminal contraction at all beat rates were shown in Fig. 4-top. The brightness decreased during the peak-systolic luminal expansion phase and increased during the end-diastolic luminal contraction phase of the pulsatile flow. The sO_2 also varied periodically for all beat rates, as shown in Fig. 4-bottom. The cyclical variations in the mBFV and sO_2 are out of phase each other, much like the PAA variations. According to Tateishi et al. [22,23], oxygen release is inhibited by RBC aggregation, so that the increase and decrease in the sO_2 can be attributed to RBC aggregation and disaggregation, respectively. This suggests that estimating regional changes in the oxygenation might provide an indirect assessment of RBC aggregation, a hemorheological phenomenon presented in many circulatory disorders.

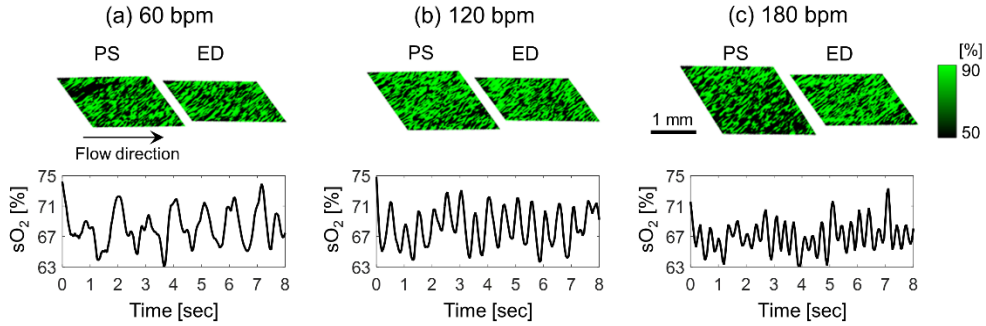

Fig. 4. (Top row) Representative images of the oxygen saturation (sO_2) at the peak-systolic luminal expansion (PS) and the end-diastolic luminal contraction (ED). (Bottom row) Cyclic variation in the mean sO_2. The left, center and right columns represent 60 (a), 120 (b) and 180 (c) bpm.

3.2 Variation of PAA and sO_2 with blood flow velocity

The variation index of the PAA (VI_{PA}) and the magnitude of cyclic variation in the sO_2 (ΔsO_2) were used to characterize the cyclic variation in the PAA and sO_2, respectively (Fig. 5). The ΔBFV increased with the beat rate such as 38 cm/s (60 bpm), 50 cm/s (120 bpm), and 52 cm/s (180 bpm). The ΔBFV is proportional to the magnitude of cyclic variation in the mean shear rate. One may expect that the magnitude of variation in the mean shear rate would be proportionate to those in both RBC aggregation and the sO_2. However, the magnitudes of the variation in both RBC aggregation (as assessed by the VI_{PA} at 750 and 850 nm) and the sO_2 (as assessed by the ΔsO_2) decreased as the magnitude of variation in the mean shear rate (as assessed by the ΔBFV) increased. In general, the VI_{PA} should increase with the ΔBFV since the aggregation/disaggregation tendency becomes larger as the shear rate varies more largely [18]. For 850 nm (red x in Fig. 5), the VI_{PA} increase is explained by the increase in the ΔBFV from 38 cm/s to 50 cm/s, which is well explained in that way. However, the VI_{PA} at 850 nm decreased at 52 cm/s of ΔBFV which is very close to 50 cm/s. This is due to the different mean mBFV between 120 and 180 bpm, even though the ΔBFV are similar each other. At

#262587 Received 5 Apr 2016; revised 13 Jun 2016; accepted 14 Jun 2016; published 23 Jun 2016

very high velocities, the mean shear rate is too high to sustain the formation of any aggregates. In addition, this phenomenon correlates with a decrease in the ΔsO_2 since the oxygen release from the non-aggregated RBCs can be more enhanced than that from the RBC aggregate [22,23].

For 750 nm (blue circle in Fig. 5), the VI_{PA} decreased with the ΔBFV from 38 cm/s to 50 cm/s, which is opposite to the case of 850 nm. This is because the ε_{HbO} is lower than the ε_{Hb} at 750 nm. For example, if more RBCs aggregate during low velocity at 120 bpm than 60 bpm, the ε_{HbO} (which is lower than ε_{Hb}) becomes more dominant at 120 bpm than 60 bpm. As a result, the PAA for aggregation can be lower at 120 bpm than 60 bpm. In contrary, if more non-aggregated single RBCs exist during high velocity at 120 bpm than 60 bpm, the ε_{Hb} (which is higher than ε_{HbO}) becomes more dominant at 120 bpm than 60 bpm, such that the PAA for non-aggregation can be higher at 120 bpm than 60 bpm. Taking into account both simultaneously occurring phenomena, the magnitude of variation in the PAA for 750 nm can be lower at 120 bpm than 60 bpm.

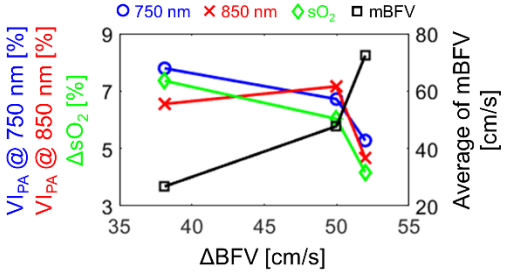

Fig. 5. The variation indices of the PAA (VI_{PA}) at 750 (blue circle) and 850 (red x) nm, the magnitude of cyclic variation in the oxygen saturation (ΔsO_2, green diamond), and the average of mean blood flow velocity (mBFV, black square) for the magnitude of cyclic variation in the mean blood flow velocity (ΔBFV).

3.3 Effect of RBC aggregation: absorber size on the PAA

As seen by the results in Figs. 2 and 4, both the PAA for all optical wavelengths (750 and 850 nm) and the sO_2 from flowing blood cyclically varied at the intervals corresponding to all beat rates (60, 120 and 180 bpm). The cyclic variation in the PAA induced by blood flow is most likely related to the cyclic variation in RBC aggregation induced by mean shear rate. Given that RBCs are the dominant absorbers in the flowing blood, the absorber size can vary periodically due to RBC aggregation and disaggregation respectively induced by the decrease and increase in the mean shear rate under pulsatile blood flow [21,32–35].

The PAA can be a function of a and μ_a, assuming that the other parameters are constant in Eq. (1). The μ_a is a function of ε_{HbO}, ε_{Hb} and sO_2 as shown in in Eq. (5), and ε_{HbO} and ε_{Hb} are dependent on the optical wavelength. If RBCs are imaged at an isosbestic point, 800 nm, then the PAA would depend only on a, because ε_{HbO} and ε_{Hb} are identical, so that the μ_a is constant. Hence, the cyclic variation in the PAA at 800 nm as shown in Fig. 6 represents the cyclic variation in the absorber size only which means the cyclic variation in the PAA due to RBC aggregates and non-aggregated single cells. However, RBCs are aggregating and disaggregating repeatedly under the pulsatile blood flow, resulting in increase and decrease in the optical absorber size, thereafter, relative increase and decrease in the sO_2, respectively [22,23]. In this way, when the pulsatile flowing blood is imaged at non-isosbestic point, RBC aggregate increases an absorber size, and might enhance the μ_a by means of increase in the sO_2. This complicated role of RBC aggregation on the PAA needs to be investigated furthermore.

#262587 Received 5 Apr 2016; revised 13 Jun 2016; accepted 14 Jun 2016; published 23 Jun 2016

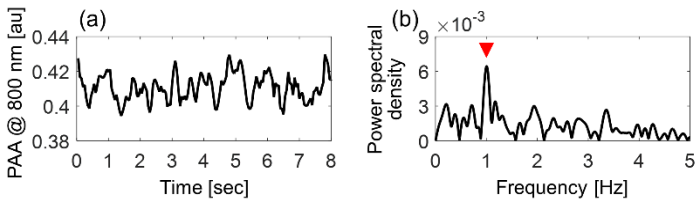

Fig. 6. Cyclic variation in the photoacoustic amplitude (PAA) at an isosbestic point, 800 nm for 60 bpm of the beat rate. (a) Time domain and (b) the power spectral density. The red mark indicates the maximal magnitude at 1 Hz.

3.4 Effect of RBC aggregation: absorption coefficient on the PAA

The size of RBC aggregates is also responsible for changing the optical absorption of the blood medium as it undergoes pulsatile flow. It was shown in the PAA increases with increasing RBC aggregation (Fig. 2). As a result, it was initially expected that the correlation between the PAA and the sO_2 at 750 nm was similar to that for 850 nm. This is explored in Fig. 7. The blue circles and red "x" symbols represent the PAA at 750 nm (left ordinate) and 850 nm (right ordinate), respectively, as a function of the sO_2 (abscissa). The minimum eigenvalues (minor axis of the ellipse) at 750 nm are significantly higher than those at 850 nm ($p = 0.038$) as shown in Fig. 7(d), whereas the maximum eigenvalues (major axis of ellipse) at 750 nm are the same as those at 850 nm for all beat rates ($p = 1$) as shown in Fig. 7(e). The correlation coefficients between the PAA and the sO_2 for 750 nm are significantly lower than those for 850 nm for all beat rates ($p = 0.003$) as shown in Fig. 7(f). In fact, the correlation coefficient for the 750 nm data reaches a maximum of ~0.6 at 60 bpm while the same coefficient at 850 nm remained close to 0.8 for all beat rates. These findings suggest that the PAA as a function of sO_2 is more linearly proportional at 850 nm than at 750 nm.

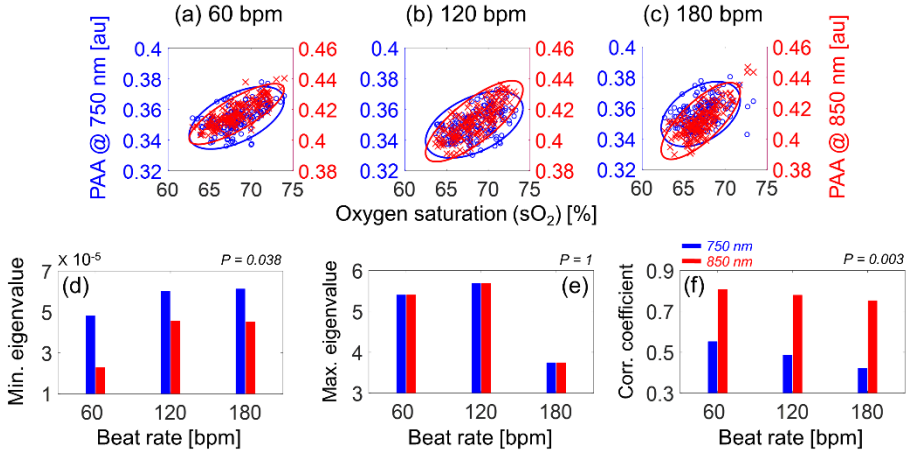

Fig. 7. Correlation between the PAA (at 750 nm as blue circles and at 850 nm as red x symbols) and the oxygen saturation at 60 (a), 120 (b), 180 (c) bpm. A 95% confidence ellipse was plotted for each case. The minimum (d) and maximum (e) eigenvalues and the correlation coefficient (f) at 750 (blue bar) and 850 (red bar) nm for all beat rates.

The μ_a of the blood samples at 750 and 850 nm were computed based on Eq. (5) and are shown in Fig. 8. The computed μ_a varied at intervals corresponding to the beat rate (Fig. 8(a)-8(c)). The cyclic variation in the computed μ_a is in phase with the PAA (Fig. 2-center row) and the sO_2 (Fig. 4-bottom row) when the blood was illuminated at 850 nm but out of phase at the 750 nm illumination. The phase difference is due to the molar extinction coefficient and concentration of hemoglobin. At 850 nm, the ε_{HbO} is larger than the ε_{Hb} regardless of RBC aggregation, and [HbO] is relatively higher during RBC aggregation than the disaggregation

#262587 Received 5 Apr 2016; revised 13 Jun 2016; accepted 14 Jun 2016; published 23 Jun 2016

state since the sO_2 is relatively higher during RBC aggregation. Hence, the μ_a in Eq. (2) at 850 nm is relatively larger during RBC aggregation than disaggregation. The opposite trends are observed at 750 nm where [Hb] is relatively higher during disaggregation than aggregation since the sO_2 is lowest. For these reasons, the cyclic variation in the computed μ_a is in phase with those in both the PAA and the sO_2 at 850 nm but out of phase at 750 nm.

The magnitudes of the cyclic variation in μ_a ($\Delta\mu_a$) at 750 nm are significantly larger than that at 850 nm for all beat rates ($p < 0.001$) because the absolute value of the difference between ε_{HbO} and ε_{Hb} at 750 nm (877.24 /cm/M) is larger than that at 850 nm (366.68 /cm/M). The significant difference of $\Delta\mu_a$ between 750 and 850 nm and the out-of-phase nature of the cyclic variations in μ_a at 750 and 850 nm can affect the PAA measured from pulsatile flowing blood. Assuming that the PAA is a function of only μ_a, the relationship between the PAA and the sO_2 shown in Fig. 7(a)-7(c) can be transformed to that between the computed μ_a and sO_2, shown in Fig. 8(d)-8(f). As predicted by Eq. (5), the slope of the computed μ_a as a function of the sO_2 is negative at 750 nm but positive at 850 nm, respectively. These results help explain the stronger linear correlation between the PAA and sO_2 at 850 nm than 750 nm (Fig. 7(f)). RBC aggregation yields increase in both the optical absorber size and the sO_2 relatively enhancing [HbO] regardless of the optical wavelength. However, even though the sO_2 increases, μ_a decreases at 750 nm since the term (ε_{HbO} - ε_{Hb}) is negative at 750 nm in Eq. (5). By examining these findings together, it can be seen that the physical interpretation of the cyclical variations in blood flow has basis on both the hemorheological phenomenon of RBC aggregation and its subsequent change in optical absorption.

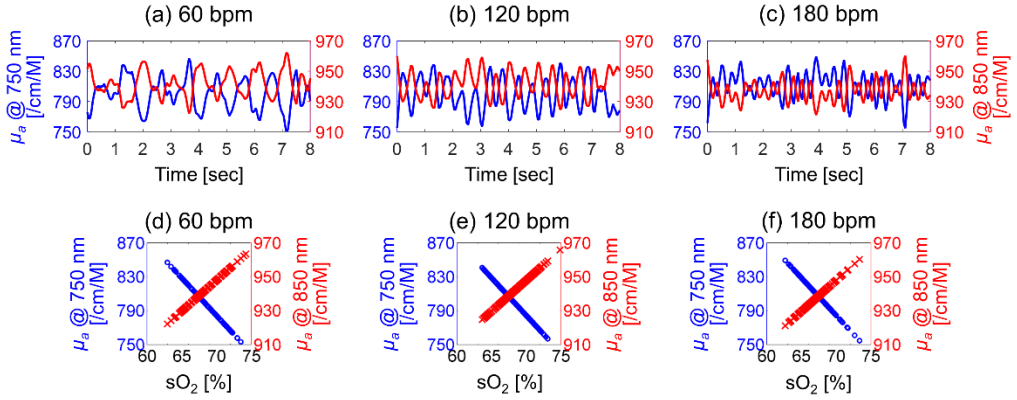

Fig. 8. Cyclic variation in the computed absorption coefficient (μ_a) at 750 (blue line) and 850 nm (red line) for 60 (a), 120 (b) and 180 (c) bpm. Correlation between the μ_a (blue circles at 750 nm and red "x" symbols at 850 nm) and the oxygen saturation (sO_2) at 60 (d), 120 (e) and 180 (f) bpm.

3.5 Potential clinical significance of this study

The present paper is the first study that considers the effect of hemodynamics on the estimation of the sO_2 by a two-wavelength method using PA imaging under pulsatile blood flow. The sO_2 measurements using photoacoustics have been demonstrated in single vessels *in vivo* using PA microscopy [9], in single RBCs in the capillary system [8], and during static RBC aggregation induced from dextran [25]. These previous studies, however, did not consider the hemodynamic relationship between RBC aggregation and the sO_2. RBC aggregation is a spontaneous hemodynamic and hemorheological phenomenon with a great deal of physiological implications. PA estimates of the sO_2 should be interpreted in conjunction knowledge of RBC aggregation and its effect on PA signals under pulsatile blood flow. Since the oxygen release is inhibited by RBC aggregation [22], there will be changes in the μ_a of RBC under pulsatile blood flow because the ratio of the oxygenated and deoxygenated hemoglobin changes as a function of RBC aggregation. Moreover, the optical

#262587 Received 5 Apr 2016; revised 13 Jun 2016; accepted 14 Jun 2016; published 23 Jun 2016

wavelength should be appropriately selected since the PAA from flowing blood a) increases and decreases with the μ_a for optical wavelegnths where ε_{Hb} is higher and smaller than ε_{HbO}, respectively, and b) increases with RBC aggregation (due to the increase in the absorber size).

The findings of this paper suggest that hemodynamics should be considered in clinical applications of PA imaging. Spontaneous oscillations in the cerebral hemodynamic signals are commonly used for monitoring cerebrovascular pathology and in functional activation research [36,37]. Hence, spontaneous [HbO] and [Hb] oscillations in subjects with cerebral infarction (CI) based on the cerebral hemodynamic signals can be analyzed for the monitoring of atherosclerosis or cerebrovascular changes [38,39]. The previous studies have suggested that the variation in the sO_2 might be a new biomarker in assessing cerebrovascular diseases in high risk subjects for CI, and the present study suggests that the sO_2 should be interpreted simultaneously with RBC aggregation under blood flow.

4. Conclusion

In this paper, the PAA and the mBFV were measured by high-frequency PA imaging at 750 and 850 nm and the Doppler velocity, respectively under pulsatile blood flow (beat rates of 60, 120 and 180 bpm). In addition, the sO_2 was computed by the two wavelength method. The PAA varied periodically out of phase with the mBFV at all beat rate demonstrating the effect of aggregate size on the PAA. Also, the sO_2 varied periodically in phase with the PAA. The PAA increases with the size of RBC aggregate and RBC aggregation inhibits oxygen release. In pulsatile flow, the aggregate size is inversely proportional to the mean shear rate. Therefore, the sO_2 can be altered by RBC aggregation under pulsatile blood flow. Moreover, the correlation between the PAA and the sO_2 was dependent on the optical wavelength of illumination since the μ_a of hemoglobin is dependent on the optical wavelength. These findings suggest that PA assessment of RBC aggregation in various circulatory disorders could be achieved through imaging of accessible human blood vessels such as the radial artery or vein. This study is a preliminary investigation opening new avenues towards understanding the hemodynamic relationship between RBC aggregation and the sO_2 through PA imaging.

Acknowledgments

This work was funded by Natural Sciences and Engineering Research Council of Canada / Canadian Institutes of Health Research - Collaborative Health Research Projects grant # 462315-2014. Funding to purchase the equipment was provided by the Canada Foundation for Innovation, the Ontario Ministry of Research and Innovation, and Ryerson University. E. Hysi is supported by a Vanier Canada Graduate Scholarship. We thank Arthur Worthington, Elizabeth Berndl, and Graham Pearson at the Department of Physics at Ryerson University for providing technical support.

#262587 Received 5 Apr 2016; revised 13 Jun 2016; accepted 14 Jun 2016; published 23 Jun 2016